

PAPER

## Effect of stress on thermal properties of AlGaN nanofilms

To cite this article: Senping Fan *et al* 2022 *Semicond. Sci. Technol.* **37** 125006

View the [article online](#) for updates and enhancements.

### You may also like

- [First-principles study of pressure-induced phase transitions, mechanical and thermodynamic properties of ThBC](#)  
Jiacheng Sun, Zhiguang Liao, Yue Zhang et al.
- [Thermal oxidation of AlGaN nanowires for sub-250 nm deep ultraviolet photodetection](#)  
Xiaodong Zhang, Tao He, Wenbo Tang et al.
- [Topology of SiO<sub>2</sub>-units and glassy network of magnesium silicate glass under densification: correlation between radial distribution function and bond angle distribution](#)  
Nguyen Hung Son, Nguyen Hoang Anh, Pham Huu Kien et al.



The Electrochemical Society  
Advancing solid state & electrochemical science & technology

243rd ECS Meeting with SOFC-XVIII

Boston, MA • May 28 – June 2, 2023

**Abstract Submission Extended  
Deadline: December 16**

[Learn more and submit!](#)

# Effect of stress on thermal properties of AlGaN nanofilms

Senping Fan<sup>1</sup>, Tianyu Yan<sup>1</sup>, Lihong Huang<sup>1</sup>, Liwen Sang<sup>2</sup> , Yang Mei<sup>1</sup>, Leiying Ying<sup>1</sup>, Baoping Zhang<sup>1</sup>  and Hao Long<sup>1,\*</sup> 

<sup>1</sup> School of Electronic Science and Engineering (National Model Microelectronics College), Xiamen University, Xiamen 361005, People's Republic of China

<sup>2</sup> International Center for Materials Nanoarchitectonics (MANA), National Institute for Materials Science (NIMS), Namiki 1-1, Tsukuba, Ibaraki 305-0044, Japan

E-mail: [longhao@xmu.edu.cn](mailto:longhao@xmu.edu.cn)

Received 11 July 2022, revised 15 October 2022

Accepted for publication 27 October 2022

Published 3 November 2022



CrossMark

## Abstract

Aluminum gallium nitride (AlGaN) nanofilms have been widely applied as active layers in ultra-violet opto-electronic devices and power electronics. Stress plays essential role in AlGaN based devices, especially in high electron mobility transistor. Therefore, it is necessary to investigate the thermal properties of AlGaN nanofilms with various stresses. In this work, biaxial stressed [0001] oriented AlGaN nanofilms were studied. The phonon dispersion, density of states, velocity and heat capacity were simulated based on the elastic theory. Thermal conductivities of AlGaN nanofilms, which was found 1 ~ 2 orders of magnitude lower than the bulk materials, were then calculated by Boltzmann transport equation. Due to the modification of phonon dispersion and increasing of group velocity by tensile stress, the thermal conductivities of AlGaN nanofilms increase from compressive stress (−15 GPa) to tensile stress (+15 GPa). Moreover, a phonon energy gap appears in AlN nanofilm of −15 GPa, which disrupts the linear relation between thermal conductivity and stresses. Our work confirmed that the stress could be promising to tune the thermal conductivity of AlGaN nanofilms.

Keywords: AlGaN nanofilms, thermal conductivity, stress, elastic theory, BTE

(Some figures may appear in colour only in the online journal)

## 1. Introduction

Composed by indium nitride, gallium nitride (GaN) and aluminum nitride (AlN), III-nitrides have been widely applied in highly efficient, high-power opto-electronic and micro-electronic devices, due to their inert chemical properties and high quantum efficiencies [1–3]. Among them, Aluminum gallium nitride (AlGaN) nanofilms with a few nanometer thicknesses have been utilized as active layers of laser diodes, high electron mobility transistor (HEMT) and UV(ultra-violet)-LEDs. Since that intense heat flux in microelectronics would degrade devices' performance and reliability [4], accurate

evaluation of AlGaN nanofilms' thermal conductivity ( $\kappa$ ) is crucial to solve the thermal dissipation issue of devices.

Typically, the  $\kappa$  of nanofilms were significantly lower than bulk counterparts since the localization of phonon in nano-thickness [5–7]. Besides, stress induced by either external force or heteroepitaxy also affect the  $\kappa$  of nanofilms. Methodology to study the  $\kappa$  of nano- or micro- films included experiments (e.g. suspended thermal bridge [5], Raman [6],  $3\omega$  [7], time domain thermal reflection [8] and laser pulse measurement [9]) and theoretical simulation. In 2005, Lui and Balandin *et al* [10] investigated the effect of Al content and temperature on  $\kappa$  of AlGaN thin films. In 2010, Tong *et al* determined the  $\kappa$  of n-type  $\text{Al}_{0.83}\text{In}_{0.17}\text{N}$  thin films to be  $4.87 \text{ W (m} \times \text{K)}^{-1}$  [11] by  $3\omega$  differential method. However, experimental reports on thermal properties of nanofilms were

\* Author to whom any correspondence should be addressed.

still rare due to the difficulty of sample preparation and complex apparatus.

Theoretical simulation of  $\kappa$  included Monte Carlo method and Boltzmann transport equation (BTE). Monte Carlo method mimics every phonon's random transportation, which needs cumbersome computational budget [12]. In recent decades, BTE method with phonon relaxation approximation was more and more popular in calculating solid thermal conductivity [13, 14]. To calculate the  $\kappa$  by BTE, phonon dispersion relation should firstly be determined. Compared with the conventional *ab initio* and molecular dynamics, elasticity theory based on Lamb wave is an easy way to derive the phonon dispersion relations [15–17]. Recently, Zhu *et al* reported the phonon dispersion and thermal properties of III-nitride nanofilms by elastic theory [18–24]. The effects of surface/interface scattering and piezoelectric on  $\kappa$  of GaN nanofilms and nanowires were investigated. Heterogeneity and prestress filed of AlN/GaN/AlN sandwich films were also calculated [23, 25]. In 2022, our group also studied the thermal properties of AlGaIn nanofilms with different Al content by elastic theory and BTE [26]. However, in our previous theoretical work, stress was also not considered yet.

Therefore, in this work, the effect of biaxial stress on thermal properties of AlGaIn nanofilm was simulated. It was shown that, the  $\kappa$  of GaN, Al<sub>0.5</sub>Ga<sub>0.5</sub>N and AlN all increase from compressive to tensile stress. A phonon bandgap appearing at –15 GPa stressed AlN nanofilms disrupted the linearity of AlN nanofilm's  $\kappa$  on stress. Our work proved that the thermal conductance of AlGaIn nanofilms could be modulated by stress fields, which may be promising for efficiently thermal dissipated AlGaIn based devices.

## 2. Phonon dispersion

In BTE model, the  $\kappa$  is integration of specific heat capacity, phonon group velocity and phonon lifetime. To derive the specific heat capacity and phonon group velocity, phonon dispersion relation should firstly be calculated. In this work, about 2 nm thick [0001] orientated quasi-2D wurtzite Al<sub>δ</sub>Ga<sub>1-δ</sub>N ( $\delta = 0, 50\%, 100\%$ ) nanofilm is considered as a slab. As shown in figure 1,  $x$  and  $y$  directions are within planar and isotropic, while  $z$  direction along [0001]. Heat flows along  $x$  direction. An isotropic stress field  $\sigma_0$  is applied along  $x$  and  $y$  directions.

According to elasticity theory, the vibration vector  $\mathbf{u}$  of slab films is calculated by elastic equation. The stress applied to nanofilms could be expressed as:

$$\sigma_{xx}^0 = \sigma_{yy}^0 = \sigma_0, \sigma_{zi}^0 = 0 \quad (i = x, y, z). \quad (1)$$

According to elastic constitutive relation, the initial strains by stress  $\sigma_0$  are:

$$\begin{aligned} u_{xx}^0 &= \frac{s_{yy} - s_{xy}}{s_{xx}s_{yy} - s_{xy}^2} \sigma_0, \quad u_{yy}^0 = \frac{s_{xx} - s_{xy}}{s_{xx}s_{yy} - s_{xy}^2} \sigma_0, \\ u_{zz}^0 &= -\frac{C_{13}}{C_{33}} u_{xx}^0 - \frac{C_{23}}{C_{33}} u_{yy}^0; \end{aligned} \quad (2)$$

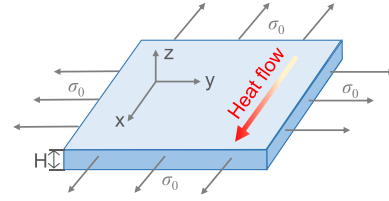


**Figure 1.** Heat flow and stress of [0001] oriented Al<sub>δ</sub>Ga<sub>1-δ</sub>N nanofilm.

where  $s_{xx} = C_{11} - \frac{C_{13}^2}{C_{33}}$ ,  $s_{xy} = C_{12} - \frac{C_{13}C_{23}}{C_{33}}$ ,  $s_{yy} = C_{22} - \frac{C_{23}^2}{C_{33}}$ ;  $C_{ij}$  is two-order elastic modulus tensor. With the interpolation of elastic modulus tensor, the planar strains  $\varepsilon_{//}$  of Al<sub>0.5</sub>Ga<sub>0.5</sub>N have a linear relation with stress:  $\varepsilon_{//} = 0.38\% [\text{GPa}^{-1}] \cdot \sigma_0$ . The typical full stress Al<sub>0.2</sub>Ga<sub>0.8</sub>N layer in Al<sub>0.2</sub>Ga<sub>0.8</sub>N/GaN HEMT has +0.49% strain and +1.25 GPa tensile stress. Under stress, the vibration equation is [27, 28]:

$$\rho^{\text{new}} \frac{\partial^2 u_i}{\partial t^2} = \frac{\partial}{\partial x_j} \left( \tilde{C}_{ijkl} \frac{\partial u_k}{\partial x_l} \right) + \sigma_0 \frac{\partial^2 u_i}{\partial x^2}; \quad (3)$$

where  $\rho^{\text{new}} = \rho [1 - (u_{xx}^0 + u_{yy}^0 + u_{zz}^0)]$  is the modified density under stress.  $\tilde{C}_{ijkl}$  is the modified fourth-order elastic modulus:

$$\begin{aligned} \tilde{C}_{ijkl} &= C_{ijkl} (1 + u_{ii}^0 + u_{jj}^0 + u_{kk}^0 + u_{ll}^0 - u_{11}^0 - u_{22}^0 - u_{33}^0) \\ &+ C_{ijklmn} u_{mn}^0; \end{aligned} \quad (4)$$

where  $C_{ijklmn}$  is sixth-order elastic modulus. By using Voigt notation, the fourth-order elastic modulus tensor  $C_{ijkl}$  can be notated into  $6 \times 6$  two-dimensional matrix  $C_{ab}$  by abbreviating the  $(ij)$  and  $(kl)$  into  $a$  and  $b$  respectively, corresponding rules of (11)→(1), (22)→(2), (33)→(3), (12)→(6), (13)→(5), and (23)→(4). The none-zero modified elastic tensor are:

$$\begin{aligned} \tilde{C}_{11} &= \tilde{C}_{22} = C_{11} (1 + 2u_{11}^0 - u_{33}^0) + (C_{111} + C_{112})u_{11}^0 + C_{112}u_{33}^0 \\ \tilde{C}_{33} &= C_{11} (1 + 2u_{11}^0 - u_{33}^0) + 2C_{112}u_{11}^0 + C_{111}u_{33}^0 \\ \tilde{C}_{13} &= \tilde{C}_{23} = C_{12} (1 + u_{33}^0) + (C_{123} + C_{112})u_{11}^0 + C_{112}u_{33}^0 \\ \tilde{C}_{12} &= C_{12} (1 + u_{33}^0) + 2C_{112}u_{11}^0 + C_{123}u_{33}^0 \\ \tilde{C}_{44} &= \tilde{C}_{55} = C_{44} (1 + u_{33}^0) + (C_{144} + C_{155})u_{11}^0 + C_{155}u_{33}^0 \\ \tilde{C}_{66} &= \frac{(\tilde{C}_{11} - \tilde{C}_{12})}{2}. \end{aligned} \quad (5)$$

When heat transports along  $x$  direction, the vibration vector  $\mathbf{u}$  is function of  $x$  and  $z$ :

$$\mathbf{u}(x, z, t) = \hat{u}(z) \exp(i(\omega t - q \cdot x)), \quad (6)$$

where  $\hat{u}(z)$  is amplitude and only related with  $z$ .  $w$  is phonon angular frequency, while  $q$  is wave vector. Substituting equation (6) into equation (3) to obtain:

$$\begin{bmatrix} \tilde{C}_{44} \frac{\partial^2}{\partial z^2} - (\tilde{C}_{11} + \sigma_0) q^2 & 0 & -iq_0 (\tilde{C}_{13} + \tilde{C}_{44}) \frac{\partial}{\partial z} \\ 0 & \tilde{C}_{44} \frac{\partial^2}{\partial z^2} - (\tilde{C}_{66} + \sigma_0) q^2 & 0 \\ -iq_0 (\tilde{C}_{13} + \tilde{C}_{44}) \frac{\partial}{\partial z} & 0 & \tilde{C}_{33} \frac{\partial^2}{\partial z^2} - (\tilde{C}_{44} + \sigma_0) q^2 \end{bmatrix} \hat{\mathbf{u}}(z) = -\rho^{\text{new}} \omega^2 \hat{\mathbf{u}}(z). \quad (7)$$

According to the Lamb wave model of slab film, the vibration modes are divided into asymmetric (AS), symmetric (SA) and shearing horizontal (SH) modes, corresponding to the symmetry of vibration vector. In SH mode,  $\mathbf{u} = (0, u_y, 0)$  has only vibration along y direction, where  $u_y = \hat{u}_y(z) \exp(i(\omega t - q \cdot x))$ . It is worth noted that the Lamb wave modes are only applicable in the situation of heat flowing along slab. When heat transfer through vertical direction, the state of phonon along z direction should be strongly

quantized with concentrated density of states. Substituting into equation (7), the vibration equation of SH mode is:

$$\tilde{C}_{44} \frac{\partial^2 \hat{u}_y}{\partial z^2} + [\rho^{\text{new}} \omega^2 - (\tilde{C}_{66} + \sigma_0) q^2] \hat{u}_y = 0. \quad (8)$$

In contrast, there are no vibration along y direction in AS and SA modes,  $\mathbf{u} = (u_x, 0, u_z)$ ,  $u_x = \hat{u}_x(z) \exp(i(\omega t - q \cdot x))$ ,  $u_z = \hat{u}_z(z) \exp(i(\omega t - q \cdot x))$ . Substituting into equation (7):

$$\begin{cases} \tilde{C}_{44} \frac{\partial^2 \hat{u}_x}{\partial z^2} - iq(\tilde{C}_{13} + \tilde{C}_{44}) q^2 \frac{\partial \hat{u}_z}{\partial z} + [\rho^{\text{new}} \omega^2 - (\tilde{C}_{11} + \sigma_0) q^2] \hat{u}_x = 0 \\ \tilde{C}_{33} \frac{\partial^2 \hat{u}_z}{\partial z^2} - iq(\tilde{C}_{13} + \tilde{C}_{44}) q^2 \frac{\partial \hat{u}_x}{\partial z} + [\rho^{\text{new}} \omega^2 - (\tilde{C}_{44} + \sigma_0) q^2] \hat{u}_z = 0 \end{cases}. \quad (9)$$

The boundary condition of stressed nanofilms is:

$$\begin{cases} \sigma_{yz} = \frac{\partial u_y}{\partial z} = 0 \\ \sigma_{xz} = \frac{\partial u_x}{\partial z} - iqu_z = 0, \sigma_{zz} = \tilde{C}_{33} \frac{\partial u_z}{\partial z} - iq\tilde{C}_{13}u_x = 0 \end{cases}. \quad (10.a) \quad (10.b)$$

Combining equations (8)–(10), the phonon dispersion relation ( $\omega \sim q$ ) could be derived by finite element differentiation. Parameters of GaN and AlN utilized in calculation are listed in table 1. Parameters of  $\text{Al}_{0.5}\text{Ga}_{0.5}\text{N}$  is derived by linear interpolation between GaN and AlN.

After calculating the phonon dispersion curve, the phonon group velocity ( $v_g$ ), density of state ( $\varrho$ ) and specific heat capacity ( $C_v$ ) can be obtained. The  $v_g$  represents the phonon energy transportation velocity:

$$v_g(\omega) = \frac{d\omega_n}{dq}, \quad (11)$$

in which the subscript n denotes the phonon branches. The phase velocity is defined as:

$$v_p(\omega) = \frac{\omega}{q}. \quad (12)$$

The density of phonon states ( $\varrho$ ) is defined as the number of phonon mode per volume and per energy at given frequency. The quasi-2D phonon  $\varrho(\omega)$  can be obtained by:

$$\varrho^{\text{SA,AS,SH}}(\omega) = \sum_n \frac{1}{2\pi H v_g(\omega)}. \quad (13)$$

$C_v$  is the integration of Bose–Einstein distribution (BED) and  $\varrho(\omega)$ :

$$C_v = k_B \int_0^{\omega_{\text{max}}} \frac{(h\omega/k_B T)^2 \exp(h\omega/k_B T)}{[\exp(h\omega/k_B T) - 1]^2} \varrho(\omega) d\omega. \quad (14)$$

The dispersion curves of SH, SA and AS modes of 2 nm stressed GaN,  $\text{Al}_{0.5}\text{Ga}_{0.5}\text{N}$  and AlN nanofilms in reduced in-plane Brillouin zone are shown in figure 2. Slopes of all modes increased from compressive to tensile stress. Moreover, with increasing the Al content, the slope of dispersion curve also increased. The first and third optical branch of SA mode show energy valleys at  $0.75 \text{ nm}^{-1}$  and  $1.75 \text{ nm}^{-1}$ . The second optical branch of AS mode shows energy valley at  $1.5 \text{ nm}^{-1}$ . It is worth noting that the Al concentration and stress have no influence on the positions of energy valleys.

**Table 1.** Parameters of GaN, Al<sub>0.5</sub>Ga<sub>0.5</sub>N and AlN [22, 29].

GaN	$C_{33}$ (GPa)	$C_{13}$ (GPa)	$C_{44}$ (GPa)	$C_{111}$ (GPa)	$C_{112}$ (GPa)
	252	129	148	-1213	-867
	$C_{123}$ (GPa)	$C_{144}$ (GPa)	$C_{155}$ (GPa)	$C_{456}$ (GPa)	$\rho$ (g/cm <sup>3</sup> )
	-253	-46	-606	-49	6.15
	<hr/>				
AlN	$C_{33}$ (GPa)	$C_{13}$ (GPa)	$C_{44}$ (GPa)	$C_{111}$ (GPa)	$C_{112}$ (GPa)
	282	149	179	-1073	-965
	$C_{123}$ (GPa)	$C_{144}$ (GPa)	$C_{155}$ (GPa)	$C_{456}$ (GPa)	$\rho$ (g/cm <sup>3</sup> )
	-61	57	-757	-9	3.26
	<hr/>				

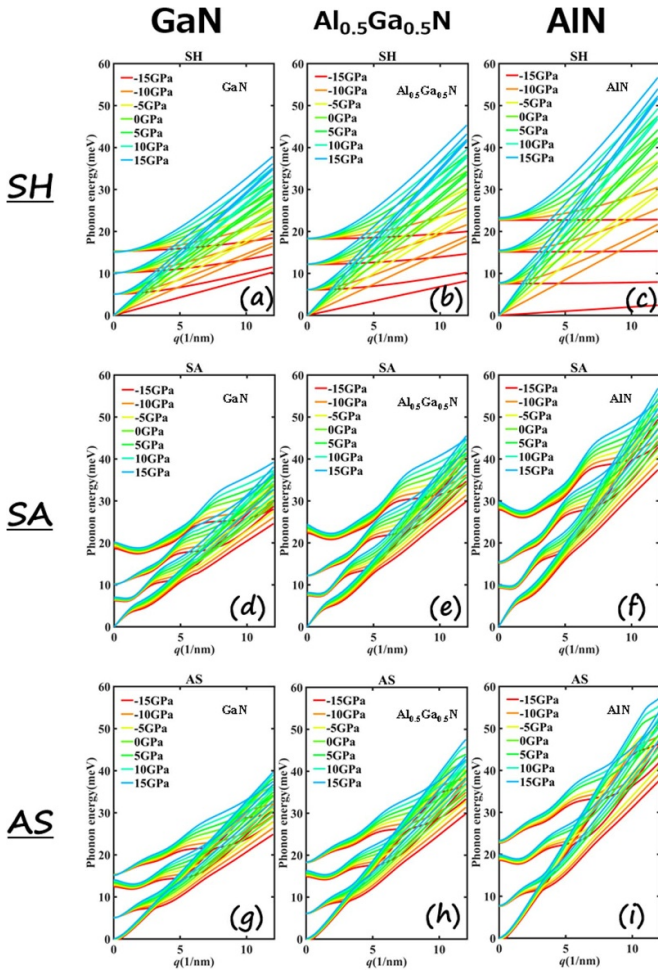
**Figure 2.** (a)–(i) SH, SA and AS phonon dispersion curves of 2 nm GaN, Al<sub>0.5</sub>Ga<sub>0.5</sub>N and AlN nanofilms.

Figure 3 shows the average group velocity ( $v_g$ ) and phase velocity ( $v_p$ ) of 2 nm thick GaN, Al<sub>0.5</sub>Ga<sub>0.5</sub>N and AlN with various stresses. The  $v_g$  decreased sharply at phonon energies corresponding to the minima of phonon dispersion slope. From compressive (−15 GPa) to tensile (+15 GPa) stress, the distribution and peak values of both  $v_g$  and  $v_p$  of GaN and Al<sub>0.5</sub>Ga<sub>0.5</sub>N blueshift, showing the increasing of Debye frequency. This is ascribed with the increasing of dispersion slope by tensile stress, which could be explained by the vibration equations (8) and (9). For instance, in SH mode, the dispersion curve ( $\omega \sim q$ ) is typically determined by parameter  $[\rho^{\text{new}}\omega^2 - (\tilde{C}_{66} + \sigma_0)q^2] / \tilde{C}_{44}$ . Since the stress  $\sigma_0$  is introduced, the eigen-frequency  $\omega$  would increase by positive  $\sigma_0$

(tension) and decreased by negative  $\sigma_0$  (compression) at same vector  $q$ . However, in case of AlN, because that a phonon bandgap appeared at SH mode in −15 GPa stress, the  $v_g$  and  $v_p$  at low energy range (0–25 meV) of −15 GPa are larger than the ones of −10 GPa (as shown in figures 3(d) and (h)), which will disrupt the  $\kappa \sim \sigma_0$  relation.

Figures 4(a)–(c) shows the density of states ( $\rho$ ) of 2 nm nitrides. The  $\rho$  increased sharply at energies corresponding to the minima of  $v_g$ . Both  $\rho$  of GaN and Al<sub>0.5</sub>Ga<sub>0.5</sub>N represent blueshift from compressive to tensile stress, which is in line with the dispersion curves. The  $\rho$  decreased at low energy range (0–25 meV) and increase at high energy range (>25 meV) by tensile stress. In AlN, the bandgap at −15 GPa make the  $\rho$  of −10 GPa higher than the one of −15 GPa without blueshift, which differed with common situations (figure 4(d)).

Figure 5 shows that the specific heat capacity ( $C_v$ ) of GaN, Al<sub>0.5</sub>Ga<sub>0.5</sub>N and AlN decreased by tensile stress. This could be explained by the blueshift of  $\rho(\omega)$  by tensile stress. Since  $C_v$  is the integration of BED and  $\rho(\omega)$ , the blueshift of  $\rho(\omega)$  and low value of BED at high energy reduce the  $C_v$ . At low temperature (<200 K), the  $C_v$  increased with temperature by square law ( $\propto T^2$ ), which is caused by the extension of BED function by temperature. The square relation differed with the cubic relation ( $\propto T^3$ ) of bulk materials [30], due to the quasi-2D character of nanofilms. Meanwhile, the  $C_v$  also decreases by Al concentration, which is consistent with our previous work [26].

### 3. BTE and thermal conductivity

According to the BTE, the thermal conductivity  $\kappa$  is integration of specific heat, group velocity and phonon lifetime  $\tau$ .

$$\kappa = \frac{1}{3} \int_0^{\omega_{\max}} C_v(\omega) v_g^2(\omega) \tau(\omega). \quad (15)$$

The phonon lifetime is related with the scattering of phonon. In this work, we considered five scattering mechanisms: Umklapp phonon-phonon scattering  $\tau_U$ , point-defect scattering  $\tau_{TP}$ , phonon-electron scattering  $\tau_{ph-e}$ , alloy disorder scattering  $\tau_{alloy}$  and boundary scattering  $\tau_B$ . Total phonon lifetime follows Matthiessen's rule by:

$$\tau^{-1} = \tau_U^{-1} + \tau_P^{-1} + \tau_{alloy}^{-1} + \tau_{ph-e}^{-1} + \tau_B^{-1}. \quad (16)$$

The Umklapp phonon-phonon scattering rate satisfies:

$$\frac{1}{\tau_U} = \frac{2\gamma^2 k_B T \omega^2 V_0^{\frac{1}{3}}}{(6\pi)^{\frac{1}{3}} M v_g v_p^2} \quad (17)$$

where Gruniesen anharmonicity parameter  $\gamma$  is 0.74 and 0.77 for GaN and AlN, respectively [10].  $k_B$  is the Boltzmann constant;  $T$  is temperature;  $V_0 = \frac{\sqrt{3}a^2c}{8}$  is the volume per atom;  $M$  is the average atom mass.

The point defect scattering rate is:

$$\frac{1}{\tau_P} = \frac{V_0 \omega^4}{4\pi v_g v_p^2} \Gamma. \quad (18)$$

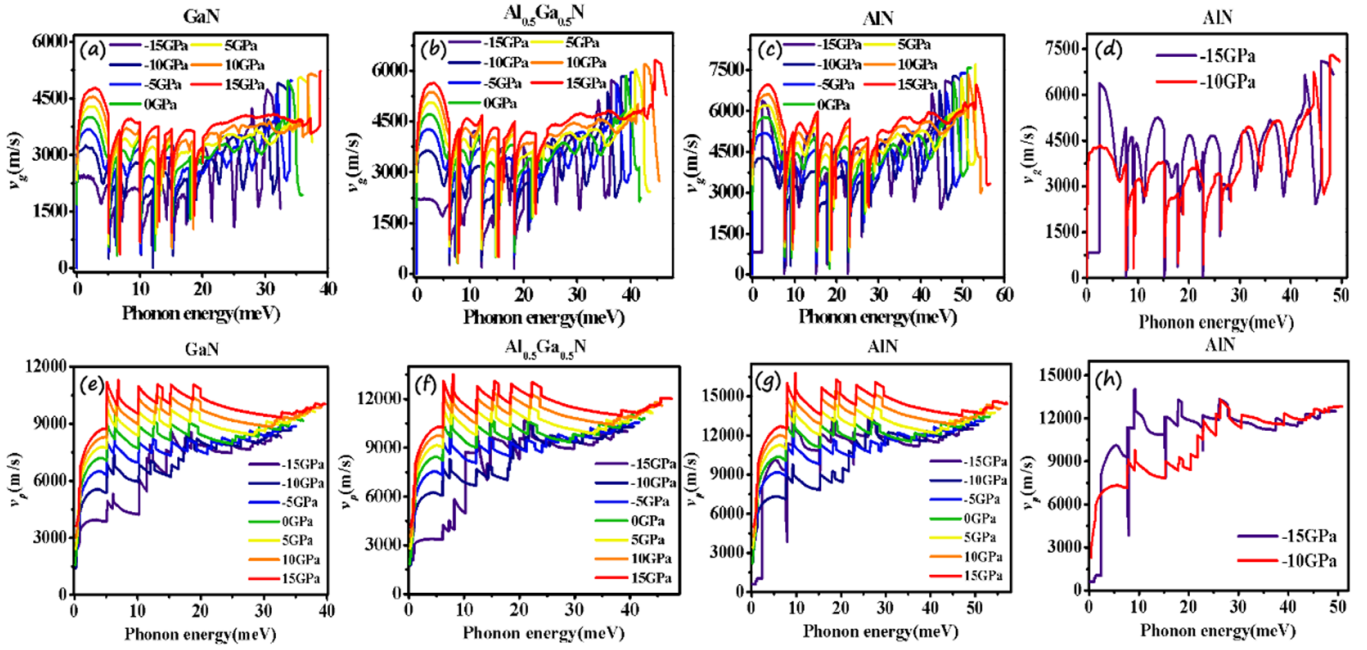


Figure 3. (a)–(d) Phonon average group velocity; (e)–(h) phonon average phase velocity of 2 nm GaN,  $Al_{0.5}Ga_{0.5}N$  and AlN.

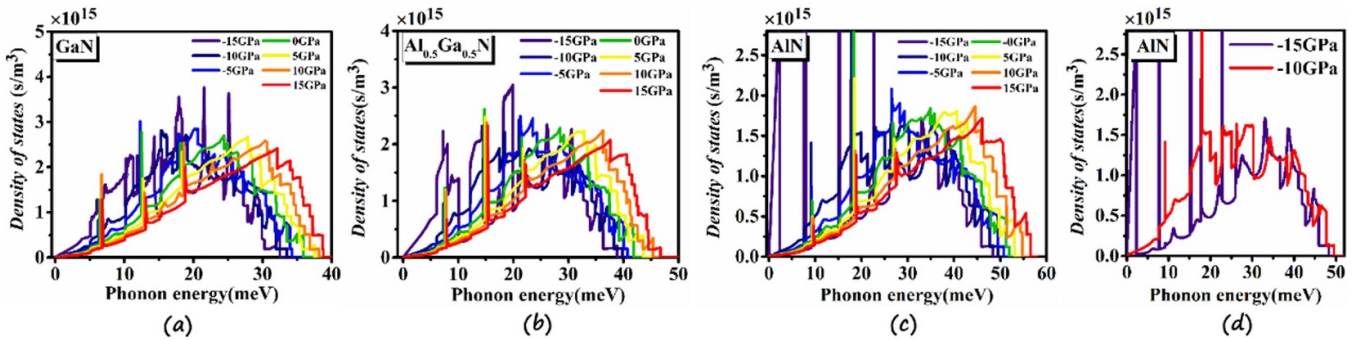


Figure 4. Phonon density of state of (a) 2 nm GaN, (b)  $Al_{0.5}Ga_{0.5}N$ , (c) AlN and (d) AlN with -15 GPa and -10 GPa.

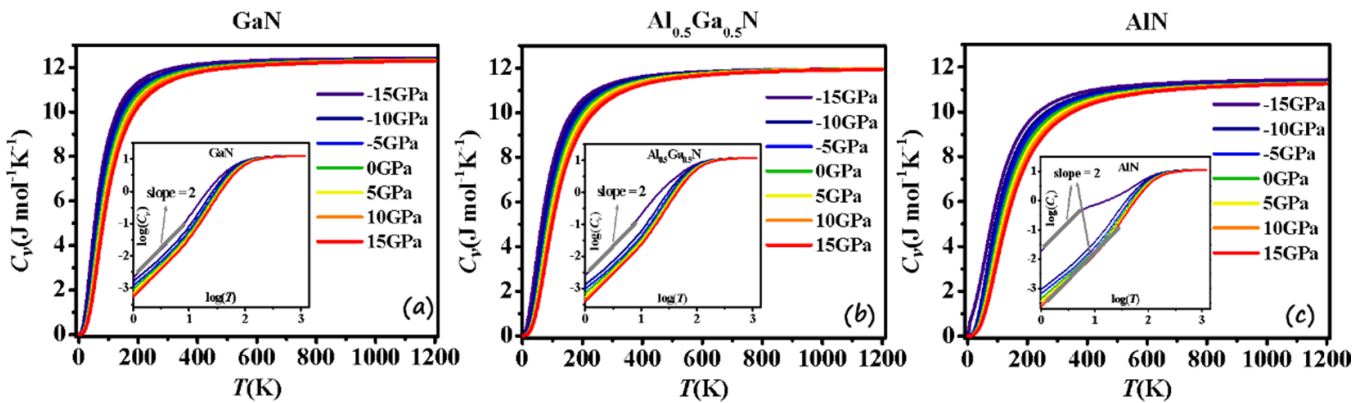


Figure 5. (a)–(c) The specific heat capacity of 2 nm GaN,  $Al_{0.5}Ga_{0.5}N$  and AlN with fitting at low temperature inset.

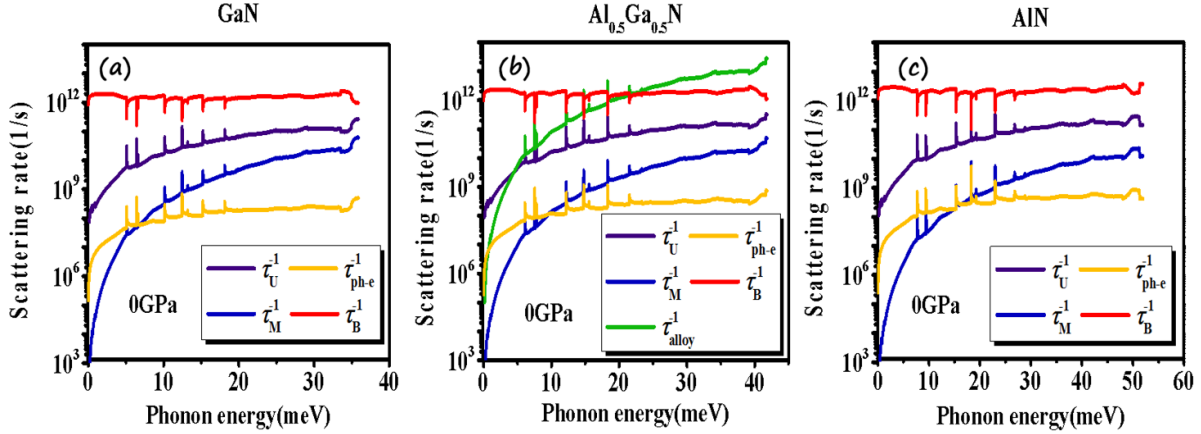


Figure 6. (a)–(c) Scattering rates of 2 nm GaN,  $\text{Al}_{0.5}\text{Ga}_{0.5}\text{N}$  and AlN at 300 K.

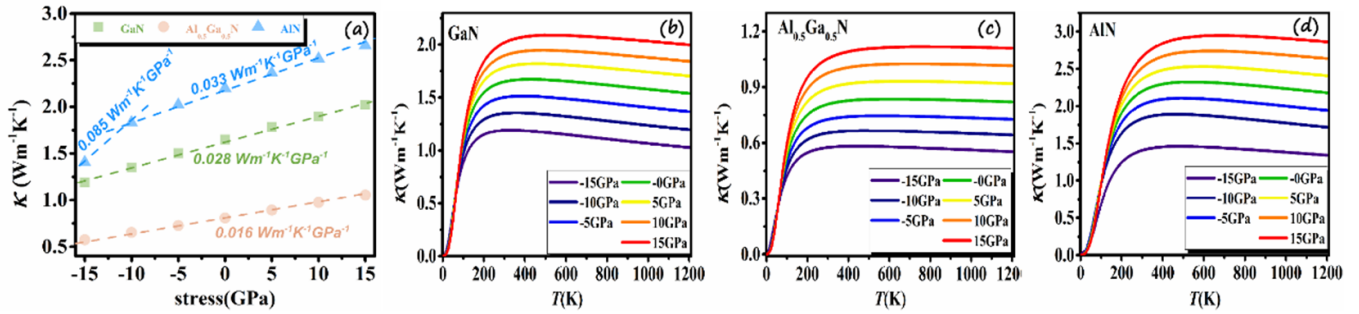


Figure 7. (a) Thermal conductivity dependence of 2 nm GaN,  $\text{Al}_{0.5}\text{Ga}_{0.5}\text{N}$  and AlN nanofilm on stress at 300 K; (b) and (c) thermal conductivity dependence of 2 nm GaN,  $\text{Al}_{0.5}\text{Ga}_{0.5}\text{N}$  and AlN on temperature.

In this work, choosing typical density ( $10^{17}$ – $10^{19}$   $\text{cm}^{-3}$ ) of point defects (carbon, hydrogen, oxygen), the point-defect scattering factor  $\Gamma$  is  $3.2 \times 10^{-4}$  and  $1.3 \times 10^{-4}$  for GaN and AlN, respectively [10].

The alloy disorder scattering rate exists in ternary AlGaIn alloy, which can be written as:

$$\frac{1}{\tau_{\text{alloy}}} = \frac{V_0 \omega^4}{4\pi v_g v_p^2} \sum_i x_i \left\{ \left[ \frac{(M_i - M)}{M} \right]^2 + \varepsilon \left[ \frac{(r_i - r)}{r} \right]^2 \right\} \quad (19)$$

where  $i$  denotes GaN or AlN.  $r$  is the average atom radius.  $\varepsilon = 39$  is a weight factor [10].

The phonon-electron scattering rate is:

$$\frac{1}{\tau_{\text{ph-e}}} = \frac{n_e \varepsilon_l^2 \omega}{\rho v_g^2 k_B T} \sqrt{\frac{\pi m^* v_g^2}{2k_B T}} \exp\left(-\frac{m^* v_g^2}{2k_B T}\right) \quad (20)$$

where  $n_e = 2 \times 10^{16}$   $\text{cm}^{-3}$  is adopted as the concentration of electrons;  $\varepsilon_l = 10.1$  eV is the deformation potential [31] and electron effective mass  $m^*$  is adopted as  $0.22 m_0$  and  $0.33 m_0$  for GaN and AlN, respectively.  $m_0$  is the vacuum electron mass.

The boundary scattering rate can be expressed as

$$\frac{1}{\tau_B} = \frac{v_g}{H}, \quad (21)$$

which is essential in nanofilms, since the thickness  $H$  is nanoscale.

As shown in figure 6, in GaN and AlN, without alloy disorder scattering, boundary scattering, due to extremely thin (2 nm) thickness, dominates the phonon scattering. Since the boundary scattering rate ( $1/\tau_B$ ) is linear proportion to group velocity, the total phonon lifetimes of GaN and AlN are determined by their group velocities. Alloy disorder scattering is another prominent scattering in  $\text{Al}_{0.5}\text{Ga}_{0.5}\text{N}$  ternary alloy.  $1/\tau_{\text{alloy}}$  is biquadrate to frequency, linearly and square inverse to the group velocity and phase velocity ( $\propto \omega^4 / (v_g \cdot v_p^2)$ ), respectively. Therefore,  $1/\tau_{\text{alloy}}$  dominated at high energy range, and decrease by tensile stress.

Integrating specific heat ( $C_v$ ), group velocity ( $v_g$ ) and scattering rate ( $\tau$ ), thermal conductivity  $\kappa$  of 2 nm nitride nanofilms were derived. As shown in figure 7,  $\kappa$  of nanofilms ( $< 3 \text{ Wm}^{-1}\text{K}^{-1}$ ) are 1–2 orders of magnitude lower than the counterparts of bulk nitride (e.g.  $70 \text{ Wm}^{-1}\text{K}^{-1}$  of GaN) [32, 35]. With modulating the stress from  $-15$  GPa compression to  $+15$  GPa tension, although the  $\rho(\omega)$  at low energy,  $C_v(\omega)$  and  $\tau_B$  decreased, the  $\kappa$  increased by tensile stress due to the enhancement of  $v_g$  and  $1/\tau_{\text{alloy}}$ , as shown in figure 7(a). Our result is consistent with aluminosilicate and magnesite material from Litovskii *et al* [34], serpentine graphene from Gao *et al* [35] and boron nitride from Zhu *et al* [36]. The  $\kappa \sim \sigma_0$  increasing slopes of GaN,  $\text{Al}_{0.5}\text{Ga}_{0.5}\text{N}$  and AlN nanofilms

are  $0.028 \text{ Wm}^{-1} \text{ K}^{-1} \text{ GPa}^{-1}$ ,  $0.016 \text{ Wm}^{-1} \text{ K}^{-1} \text{ GPa}^{-1}$  and  $0.033 \text{ Wm}^{-1} \text{ K}^{-1} \text{ GPa}^{-1}$ , respectively, originating from evolution of mass density, elastic modulus and scattering rates. It is worth noting that the  $\kappa \sim \sigma_0$  slope of AlN from  $-15 \text{ GPa}$  to  $-10 \text{ GPa}$  ( $0.085 \text{ Wm}^{-1} \text{ K}^{-1} \text{ GPa}^{-1}$ ) is pretty larger than the  $0.033 \text{ Wm}^{-1} \text{ K}^{-1} \text{ GPa}^{-1}$  of other stresses, which is ascribed with the phonon bandgap in SH mode.

Temperature dependent thermal conductivities ( $\kappa \sim T$ ) of nanofilms were shown in figures 7(b)–(d).  $\kappa$  increased with temperature until about  $200 \text{ K}$  and then saturated ( $\text{Al}_{0.5}\text{Ga}_{0.5}\text{N}$ ) or slightly decreased ( $\text{GaN}$  and  $\text{AlN}$ ). The increasing of  $\kappa$  at low temperature originated from the increasing of  $C_v$ , while the slight descending ( $\text{GaN}$  and  $\text{AlN}$ ) at high temperature came from activation of  $1/\tau_U$ , which is however screened by alloy disorder in  $\text{Al}_{0.5}\text{Ga}_{0.5}\text{N}$ . The bandgap of  $-15 \text{ GPa}$  AlN nanofilm made the  $\kappa$  keeping constant at high temperature, unlike the situation of other stress.

#### 4. Conclusion

In this work, dependence of  $2 \text{ nm}$  AlGa<sub>N</sub> nanofilms' thermal properties (phonon dispersion, density of state, specific heat and thermal conductivity) on stress was studied by elasticity theory and BTE. It was shown that all the thermal conductivities of GaN,  $\text{Al}_{0.5}\text{Ga}_{0.5}\text{N}$  and AlN nanofilms increased with tensile stress by different  $\kappa \sim \sigma_0$  slopes. Phonon bandgap at  $-15 \text{ GPa}$  stress changes the trends of  $\kappa \sim \sigma_0$  relation of AlN nanofilm. Our work proves that the stress could be a promising way to design and modulate the thermal conductivity of AlGa<sub>N</sub> nanofilms and thus the heat dissipation of AlGa<sub>N</sub> based opto-electronic devices.

#### Data availability statement

All data that support the findings of this study are included within the article (and any supplementary files).

#### Acknowledgments

The work was supported by the National Natural Science Foundation of China (No. 62174140), the Youth Innovation Foundation of Xiamen, China (3502Z20206055) and the Fundamental Research Funds for the Central Universities (20720220077).

#### ORCID iDs

Liwen Sang  <https://orcid.org/0000-0003-0946-1025>  
Baoping Zhang  <https://orcid.org/0000-0001-9537-5179>  
Hao Long  <https://orcid.org/0000-0002-7057-7214>

#### References

- [1] Fichter F 1907 Über aluminiumnitrid *Z. Anorg. Chem.* **54** 322–7
- [2] Fischer F and Schröter F 1910 Neue Untersuchungen über die Verbindungsfähigkeit des Argons *Ber. Dtsch. Chem. Ges.* **43** 1442–54
- [3] Johnson W C, Parson J B and Crew M C 1932 Nitrogen compounds of gallium. III *J. Phys. Chem.* **36** 2651–4
- [4] Sang L 2021 Diamond as the heat spreader for the thermal dissipation of GaN-based electronic devices *Funct. Diam.* **1** 174–88
- [5] Shi L, Li D, Yu C, Jang W, Kim D, Yao Z, Kim P and Majumdar A 2003 Measuring thermal and thermoelectric properties of one-dimensional nanostructures using a microfabricated device *J. Heat Transfer* **125** 881–8
- [6] Luo Z, Maassen J, Deng Y, Du Y, Garrelts R P, Lundstrom M S, Ye P D and Xu X 2015 Anisotropic in-plane thermal conductivity observed in few-layer black phosphorus *Nat. Commun.* **6** 1–8
- [7] Cahill D G, Katiyar M and Abelson J 1994 Thermal conductivity of a-Si:H thin films *Phys. Rev. B* **50** 6077
- [8] Sood A, Xiong F, Chen S, Cheaito R, Lian F, Asheghi M, Cui Y, Donadio D, Goodson K E and Pop E 2019 Quasi-ballistic thermal transport across MoS<sub>2</sub> thin films *Nano Lett.* **19** 2434–42
- [9] Bozlar M, He D, Bai J, Chalopin Y, Mingo N and Volz S 2010 Carbon nanotube microarchitectures for enhanced thermal conduction at ultralow mass fraction in polymer composites *Adv. Mater.* **22** 1654–8
- [10] Liu W and Balandin A A 2005 Thermal conduction in  $\text{Al}_x\text{Ga}_{1-x}\text{N}$  alloys and thin films *J. Appl. Phys.* **97** 073710
- [11] Tong H, Zhang J, Liu G, Herbsommer J A, Huang G S and Tansu N 2010 Thermoelectric properties of lattice-matched AlInN alloy grown by metal organic chemical vapor deposition *Appl. Phys. Lett.* **97** 112105
- [12] Suzuki A, Watanabe T, Kamakura Y and Kamioka T 2014 Full-scale whole device EMC/MD simulation of Si nanowire transistor including source and drain regions by utilizing graphic processing units *Proc. 2014 Int. Conf. on Simulation of Semiconductor Processes and Devices (SISPAD)* (IEEE)
- [13] McGaughey A J and Kaviani M 2004 Quantitative validation of the Boltzmann transport equation phonon thermal conductivity model under the single-mode relaxation time approximation *Phys. Rev. B* **69** 094303
- [14] Martin P, Aksamija Z, Pop E and Ravaioli U 2009 Impact of phonon-surface roughness scattering on thermal conductivity of thin Si nanowires *Phys. Rev. Lett.* **102** 125503
- [15] Zou J, Lange X and Richardson C 2006 Lattice thermal conductivity of nanoscale Al N/Ga N/Al N heterostructures: effects of partial phonon spatial confinement *J. Appl. Phys.* **100** 104309
- [16] Bannov N, Aristov V, Mitin V and Strosio M A 1995 Electron relaxation times due to the deformation-potential interaction of electrons with confined acoustic phonons in a free-standing quantum well *Phys. Rev. B* **51** 9930
- [17] Balandin A and Wang K L 1998 Significant decrease of the lattice thermal conductivity due to phonon confinement in a free-standing semiconductor quantum well *Phys. Rev. B* **58** 1544
- [18] Zhu L and Ruan H 2014 Influence of prestress fields on the phonon thermal conductivity of GaN nanostructures *J. Heat Transfer* **136** 102402

- [19] Luo H and Zhu L 2015 Effects of surface stress on the phonon properties in GaN nanofilms *J. Appl. Mech.* **82**
- [20] Hou Y and Zhu L-L 2016 Influence of surface scattering on the thermal properties of spatially confined GaN nanofilm *Chin. Phys. B* **25** 086502
- [21] Zhu L and Luo H 2016 On the role of piezoelectricity in phonon properties and thermal conductivity of GaN nanofilms *Theor. Appl. Mech. Lett.* **6** 277–81
- [22] Zhu L and Luo H 2016 Phonon properties and thermal conductivity of GaN nanofilm under prestress and surface/interface stress *J. Alloys Compd.* **685** 619–25
- [23] Wang J, Zhu L and Yin W 2018 Effects of heterogeneity and prestress field on phonon properties of semiconductor nanofilms *Comput. Mater. Sci.* **145** 14–23
- [24] Zhu L, Tang X, Wang J and Hou Y 2019 Modeling phonon thermal conductivity in spatially confined GaN nanofilms under stress fields and phonon surface scattering *AIP Adv.* **9** 015024
- [25] Zhang S, Tang X, Ruan H and Zhu L 2019 Effects of surface/interface stress on phonon properties and thermal conductivity in AlN/GaN/AlN heterostructural nanofilms *Appl. Phys. A* **125** 732
- [26] Huang L, Fan S, Sang L, Mei Y, Ying L, Zhang B and Long H 2022 Thermal conductivity and phonon scattering of AlGaIn nanofilms by elastic theory and Boltzmann transport equation *Semicond. Sci. Technol.* **37** 055003
- [27] Osetrov A, Fröhlich H-J, Koch R and Chilla E 2000 Acoustoelastic effect in anisotropic layered structures *Phys. Rev. B* **62** 13963
- [28] Pao Y-H and Gamer U 1985 Acoustoelastic waves in orthotropic media *J. Acoust. Soc. Am.* **77** 806–12
- [29] Łepkowski S and Gorczyca I 2011 *Ab initio* study of elastic constants in  $\text{In}_x\text{Ga}_{1-x}\text{N}$  and  $\text{In}_x\text{Al}_{1-x}\text{N}$  wurtzite alloys *Phys. Rev. B* **83** 203201
- [30] Danilchenko B, Paszkiewicz T, Wolski S, Jeżowski A and Plackowski T 2006 Heat capacity and phonon mean free path of wurtzite GaN *Appl. Phys. Lett.* **89** 061901
- [31] Zou J 2010 Lattice thermal conductivity of freestanding gallium nitride nanowires *J. Appl. Phys.* **108** 034324
- [32] Anaya J, Rossi S, Alomari M, Kohn E, Tóth L, Pécz B and Kuball M 2015 Thermal conductivity of ultrathin nano-crystalline diamond films determined by Raman thermography assisted by silicon nanowires *Appl. Phys. Lett.* **106** 223101
- [33] Cuffe J et al 2015 Reconstructing phonon mean-free-path contributions to thermal conductivity using nanoscale membranes *Phys. Rev. B* **91** 245423
- [34] Litovskii E Y, Kushnirskii G and Fedina I 1983 Influence of compressive stress on the thermal conductivity of aluminosilicate and magnesite materials *Strength Mater.* **15** 992–4
- [35] Gao Y, Yang W and Xu B 2016 Unusual thermal conductivity behavior of serpentine graphene nanoribbons under tensile strain *Carbon* **96** 513–21
- [36] Zhu T and Ertekin E 2015 Resolving anomalous strain effects on two-dimensional phonon flows: the cases of graphene, boron nitride, and planar superlattices *Phys. Rev. B* **91** 205429